Surface crack network detection on MgO-based refractory castable by digital image correlation

R G M Saracura, R B Canto, V C Pandolfelli, N. Schmitt, François Hild

Surface crack network detection on MgO-based refractory castable by digital image correlation

R. G. M. Saracura[1], R. B. Canto[1], V. C. Pandolfelli[1], N. Schmitt[2,3], F. Hild[2]

[1]Department of Materials Engineering (DEMa), Federal University of São Carlos (UFSCar), Brazil
[2]Laboratoire de Mécanique et Technologie (LMT-Cachan), ENS Cachan / CNRS / PRES UniverSud Paris, France
[3]Université Paris-Est Créteil Val de Marne (UPEC), France

Abstract

A preliminary application of the digital image correlation (DIC) is presented aiming to detect and analyze crack networks which are induced by stresses arising during curing and drying (CD) of MgO containing refractory castable slabs. Surface images of castable samples placed in a specially designed climatic chamber were recorded over the CD stages with a digital camera and processed by the DIC technique to measure the displacement fields. Post-processing DIC results were carried out to estimate the length, orientation and opening of cracks in the networks. The methodology is highlighted and first experimental results are shown pointing out its future potential to better understand the effect of the physical aspects (particle size, chemical analysis, temperature, etc.) and the structural ones (slab shape and size) on processing and performance of advanced refractory castables.

Keywords: Crack detection, DIC, Refractory castable.

1. Introduction

Extending the lifetime and increasing the refractory working temperature resistance are two key objectives to improve quality and reduce costs for the producer and end-user [1]. A way to fulfill these aims is by designing the composition of a high temperature castable in order to control the cracking formation during curing and drying (CD) stages, as its chemical corrosion is faster when damaged hot surfaces are in contact with molten metals or oxides (e.g., slag). Conversely, crack networks can also be beneficial as they provide thermal stress relaxation.

Developing novel compositions of castables containing both alumina and magnesia particles leading to reduced microcracking after the CD stages is a continuous demand of the refractory producers. The hydration of magnesia particles is a key issue as it results in local volume expansion, inducing inner stresses and crack initiation [2]. In order to better understand the deformation associated to the in-situ phase transformation, an experimental device and digital image processing technique have been developed to quantify the crack network features. These aspects are highlighted in this paper and some preliminary results are presented.

Digital Image Correlation (DIC) will be used to detect the crack formation as this optical full-field displacement measurement technique has been applied to many areas of material sciences and mechanical engineering [3,4]. It is a suitable method to estimate strains at the surface of refractories

subjected to stresses, based on digital image acquisition of undeformed and deformed configurations, thus providing the displacement field measurement. In recent years, it has been used to characterize refractory products (i.e., materials and structures) at the lab scale [5,6] and also in other domains in order to detect crack initiation and propagation under thermal fatigue [3,7] or drying of concrete [8].

2. Experimental procedure

A high alumina castable containing 6 wt% of high surface area (SA) magnesia was used. The raw material composition and the aggregate size are presented in Table 1. The castable was prepared in a paddle mixer after adding 5.5 wt% of water (based on the dry content) and homogenized for 10 min. The resulting suspension was cast under vibration into prismatic molds (150 mm × 25 mm × 25 mm).

Table 1: Composition of the raw materials for Al_2O_3-MgO based castable

Raw materials	Tabular alumina (d ≤ 6 mm)	Reactive alumina (CL370)	Caustic magnesia SA = 24.57 $m^2 g^{-1}$	Tabular alumina (d < 45 μm)
wt%	81	7	6	6

After casting, the samples were firstly stored in a climatic chamber (Vöetsch 2020, Germany) kept for 3 h at 50 ºC and 80 % relative humidity. After that they were withdrawn out of the molds and B_4C dust was sprayed over their surfaces to create a gray scale speckle pattern for the DIC measurements. The samples were then stored up to 24 h in a specially designed climatic chamber under the same environmental conditions as the previous step. Each sample was placed on the top of thin metal rods so that all the castables´ surfaces were in contact with moist air.

2.1. In-house climatic chamber and digital image acquisition

A specific climatic chamber, comprising digital cameras and light spots to record the surface changes of castable slabs, has been designed to recreate the environmental conditions on a lab scale (i.e., temperature T and relative humidity RH) of in-service CD castable steps (Fig. 1). The images acquired were stored and the displacement field measurements were carried out by DIC. An additional post-processing tool was developed to quantify the crack network generated during the process. The chamber is equipped with an electrical resistance element and a hydrolysis humidifier with an N322RHT Novus temperature and relative humidity controller. In order to keep temperature and humidity homogeneous inside the chamber, four fans were used and placed under the sample stand to prevent direct airflow over the samples.

Glass windows enable visualization and recording of the lateral and top surfaces of the castable slab with the help of digital cameras placed outside and in front of each window. Fog and condensate water deposition on the glass windows was prevented by a hot air blower that was regularly activated (i.e., 1 min every 10 min) as shown in Fig. 1.

A high definition (15.1 Mpixel) Canon 50D digital camera with a Canon macro 100 mm lens was used (Canon Inc., Japan). Homogeneous and continuous lighting of the sample surfaces was provided using an LED based system. The images were recorded every 15 min with a f/2.8 aperture and a exposure time of 100 ms. The typical size of the Region of Interest (ROI) was about 350×2100 pixels, where each pixel size corresponds to 70 μm.

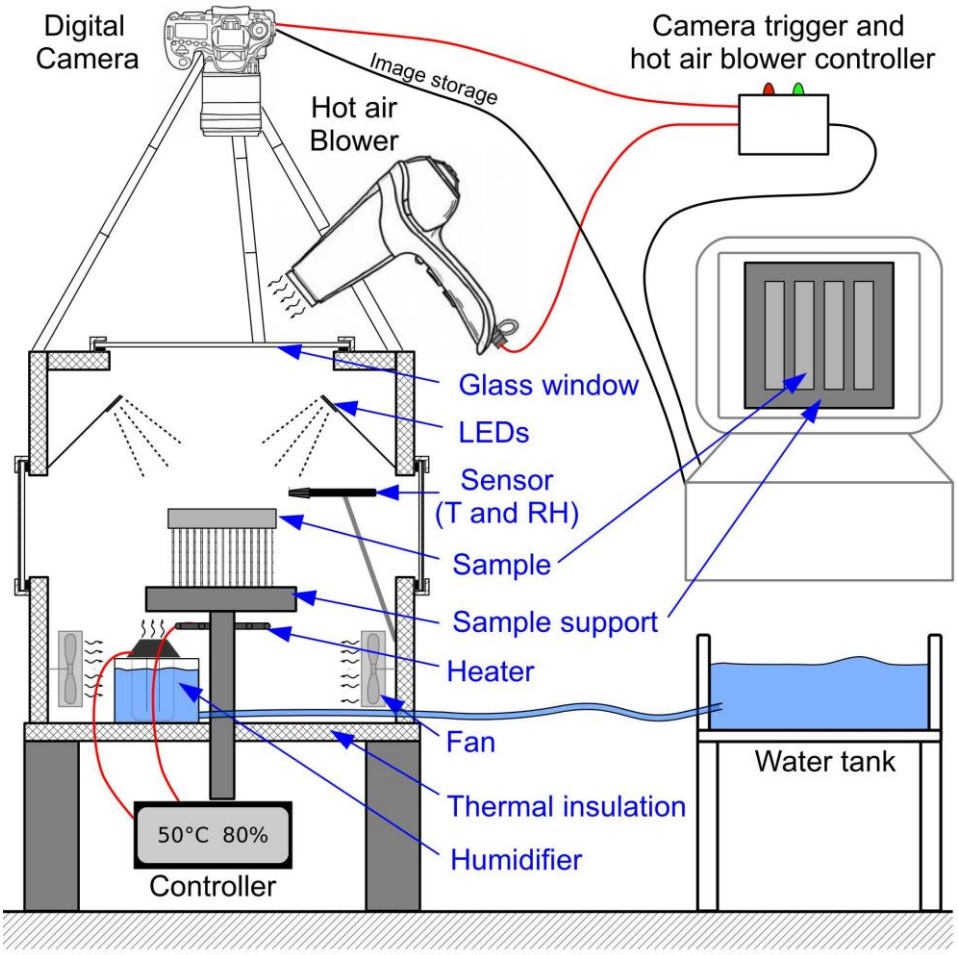

Figure 1: Experimental setup for the castable evaluations

2.2. DIC technique and estimation of crack network features

DIC provides the measurement of a displacement field $\mathbf{u}(\mathbf{x})$ by recording random B_4C speckle patterns sprayed on the surface of samples [3, 4]. For each image, the ROI is described by a scalar function that represents the gray intensity of each $\mathbf{x}$ pixel. For the initial configuration $i = 0$, the picture is denoted by $f(\mathbf{x})$ and corresponds to the first image after demolding and placing the slab in the climatic chamber (i.e., approximately 3 h after casting). The correlation consists of evaluating the similarity between f and the picture in the deformed g configuration, by minimizing the error function over the region of interest Ω (Eq. 1).

$$\eta^2 = \int_{\Omega} [f(\boldsymbol{x}) - g(\boldsymbol{x} + \boldsymbol{u}(\boldsymbol{x}))]^2 \quad (1)$$

After minimizing this error function, the residual of the correlations are obtained. These residuals are associated with the remaining difference in a pixel gray level that cannot be understood just by analyzing the estimated displacement field. Thus, when a discontinuity on the surface of the material is generated, a local change in the gray level can be computed as depicted in Fig. 2a. Therefore, the analysis of the residual of the correlations can be a way to detect the presence of cracks.

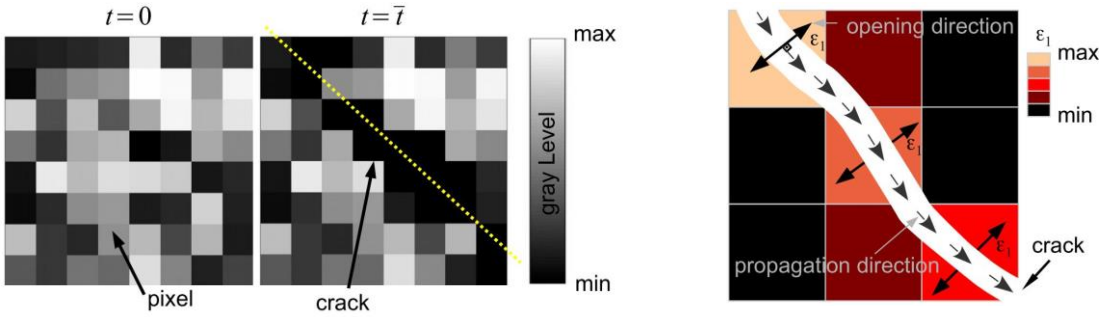

(a) (b)

Figure 2: Schematic representation of crack detection, (a) by the residuals of the correlation illustrated herein by the black squares in an 8 by 8 pixel Q4 element and (b) by the maximum principal strain highlighted by a region with a set of nine elements containing the crack.

The Correli-Q4 software [9] used in this study, assumes that the displacement field **u** is split as a set of finite element shape functions. The image is partitioned into pixels and 4-noded quadrilateral (Q4) elements are chosen with bilinear displacement interpolations. Each element contains $n \times n$ pixels and its size, ℓ, is given either in pixels (i.e., $\ell = n$) or in metric dimension. The in-plane strain tensor $\epsilon(\mathbf{x})$ is directly derived from the mean displacement gradient per Q4 element.

When the pixel size and the Q4 element one are small enough, the DIC records local heterogeneities induced either by strain localization or displacement discontinuities [9,10]. If the latter occurs for a particular element, the mean strain tensor ϵ is expressed by two terms that are added together: the first one represents the mean strain of the unbroken region and the second is a result of the average crack opening displacement $\Delta\mathbf{u}$. Consequently, the rapid change in the strain tensor, and mainly its maximum principal strain component $\epsilon_1(\mathbf{x})$, enables the detection of cracks created inside the element. As cracks generally propagate perpendicularly to the ϵ_1-direction, it is suitable to compute both the maximum principal strain field $\epsilon_1(\mathbf{x})$ and the eigenvector one $\mathbf{v}_1(\mathbf{x})$, the latter being orthogonal to the crack plane (Fig. 2b). On the surface, the direction of crack propagation is thus given by the $\mathbf{v}_2(\mathbf{x})$ eigenvector; which is orthogonal to $\mathbf{v}_1(\mathbf{x})$; and the angle $\theta(\boldsymbol{x}) = (\widehat{\boldsymbol{x}, \boldsymbol{v_2}})$.

The DIC results are post-processed with a routine developed in Matlab™ that characterizes the crack network created during the test, using the maximum principal strain component (Fig 2b) technique. The series of Q4 elements that comprises a digital image named "i" is divided into groups of elements. The G_{nci} group contains elements for which the maximum principal strain ϵ_1 at time t_i is less than a threshold strain $\epsilon^\star$ and defines the region of the image where no crack has been detected. The G_{ci} group contains the k_i elements for which the condition $\epsilon_1(t \leq t_i) \geq \epsilon^\star$ was fulfilled at least once, indicating the crack presence likelihood

For this element with a size ℓ, the crack length c_{ki} is given by Eq. 2, as shown in Fig. 3. The crack opening Δu_{ki} can be calculated by Eq. 3.

$$c_{ki} = \frac{\ell}{\sin \alpha_{ki}} \tag{2}$$

$$\Delta u_{ki} = \ell . \epsilon_{1_{ki}} \tag{3}$$

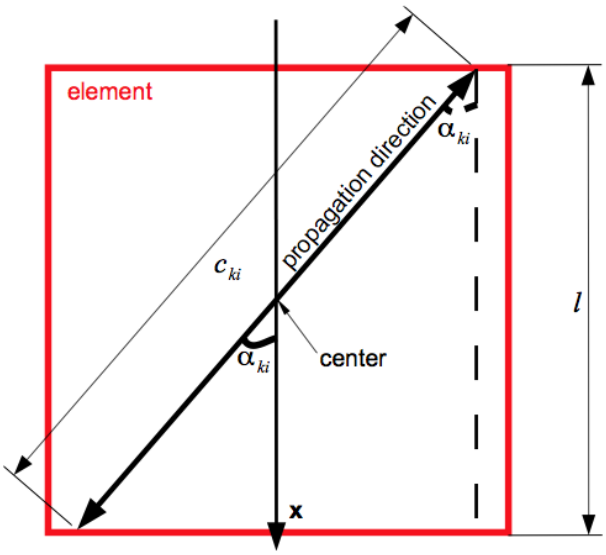

Figure 3: Element representation for crack length evaluation.

Lastly, the total crack network length, c, (Eq. 4) and the surface crack density, χ, (Eq. 5) are evaluated,

$$c = \sum_i c_{ki} \tag{4}$$

$$\chi = \frac{c}{S_{ROI}} \tag{5}$$

where, S_{ROI} is the surface´s ROI and the average opening displacement, Δu, is obtained by an accumulation over the number of elements containing cracks.

Numerous computations have been carried out to validate this method and an influence of the discretization (i.e., element size ℓ) on the results was found. The best ones were attained for $\ell = 8$ pixels and will be used in the following section. The effect of the threshold $\epsilon^\star$ was also estimated as the crack density and the time of first inception strongly depends on it. The value of $\epsilon^\star$ was chosen to be the lowest one for which no unexpected fluctuations were observed at the beginning of the total crack length profile.

3. Results and discussion

The experimental results of a slab subjected to the CD stages were analyzed after recording the images on the lateral surface. Figure 4a-b shows the measured displacements field for a given time of the experiment. The maximum principal strain field is shown in Figure 4c and the residual of the correlations one in Figure 4d.

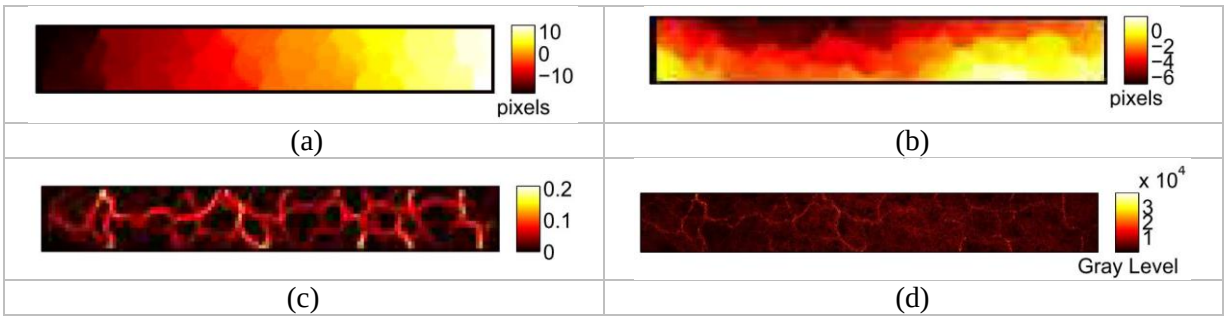

Figure 4: Longitudinal (a) and vertical (b) displacement fields expressed in pixels. Maximum principal strain field (c) and gray level residuals of correlation (d) on the lateral surface of a castable slab.

Figure 5a shows the change of the crack pattern obtained after computing the residual field for four times. The residual of the correlations indicate areas where the continuity hypothesis is not fulfilled (i.e., induced by the presence of cracks). Figure 5b depicts the change of the average level of the residuals of correlation over the whole region of interest. A gradual degradation is observed, which highlights the presence of more cracks as time progresses. Nevertheless, the resulting profile does not indicate the continous and smooth evaluation of the cracking growth.

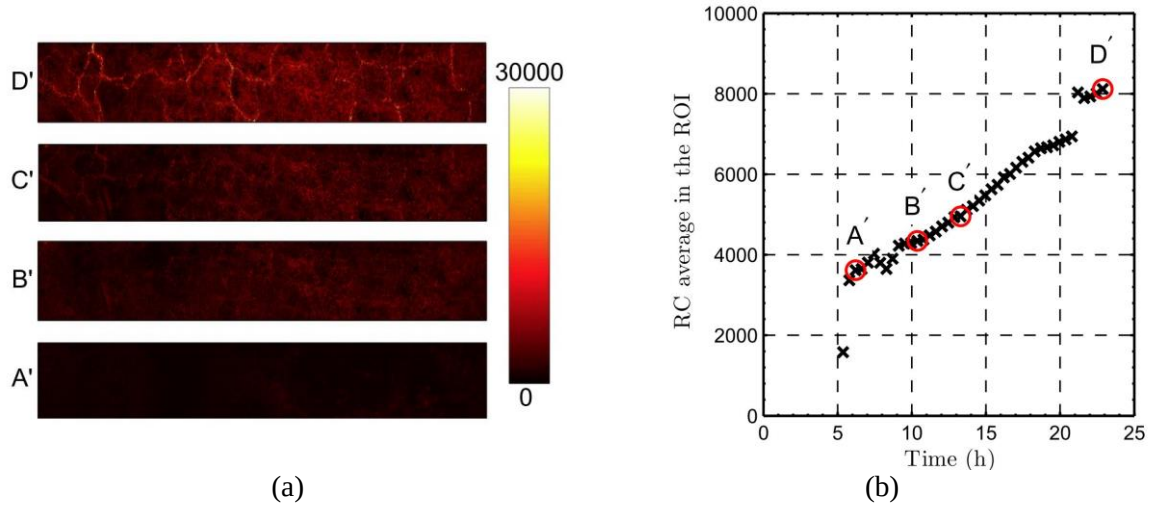

Figure 5: (a) Crack pattern evolution highlighted by the analysis of the residuals of correlation and (b) average level versus time on the lateral surface of a castable slab.

Figure 6a points out the change of the crack pattern obtained after computing the maximum principal strain field four times, whereas Fig. 6b shows the evolution of the average maximum principal strain (AMPS) over the whole region of interest. It is possible to highlight that AMPS resulted in a smoother data curve for the cracking evaluation process (Fig. 6b) when compared to that based on the residuals of correlation (Fig 5b). From the beginning of the image acquisition (i.e., 3 h after casting) until the time corresponding to point A, the strain field is nearly uniform and no crack is detected, as the hydration of MgO particles of the polycrystalline material is limited to a fine surrounding layer. The associated local expansion is partially absorbed by the nearby porosity resulting in a low macroscopic strain level, nearly undetectable at the observed scale (i.e., the pixel size 70 μm is much larger than the size of reactive MgO and Al_2O_3). After 10.4 h (point B), the AMPS is approximately equal to 0.01. During this period, the hydration progresses and the associated slab swelling is heterogeneous, most likely higher near its surface than in the bulk. Macroscopic cracks are

formed as a result of the excessive stresses at the surface of the slab, splitting the ROI into sound domains separated by the cracks. Nevertheless, at this stage their opening remains very small. After 13.3 h (point C) the AMPS value increases to 0.03 and the principal strains are much higher in some regions. The crack density also increases as new ones are created in the sound domains. After nearly 24 h (point D), some cracks significantly increased inside the slab and the high strain is associated to the crack opening.

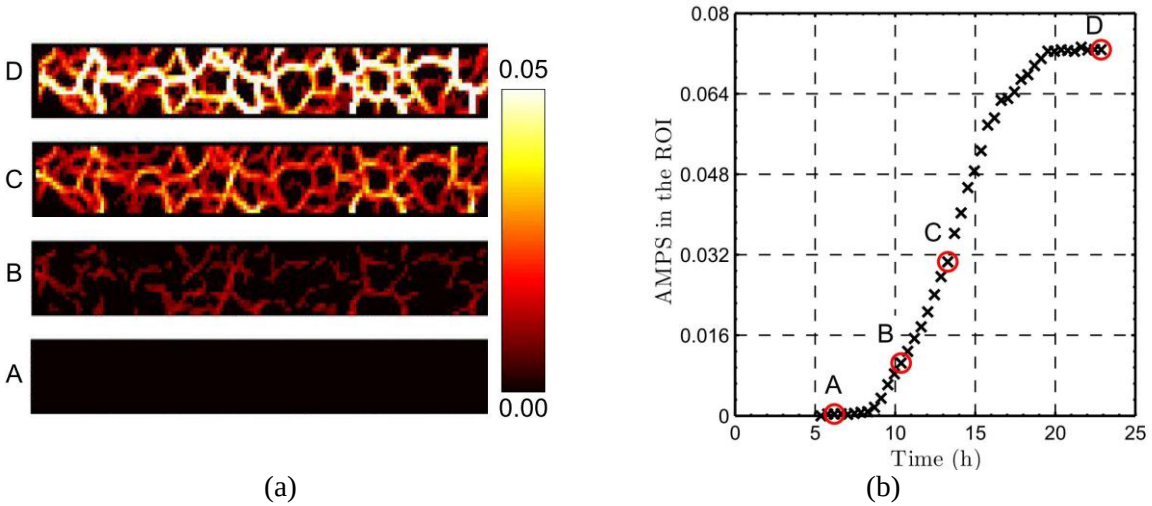

(a) (b)

Figure 6: (a) Crack pattern evolution highlighted by the analysis of the maximum principal strain field and (b) average maximum principal strain (AMPS) versus time on the lateral surface of a castable slab.

Figure 7a presents the time change effect on the surface crack density (χ) and Fig. 7b highlights the average crack opening (Δu) when the proposed method to identify the crack network was applied using $\epsilon^{\star}= 0.005$. Δu is continuously increasing over the CD stages and is directly correlated with the AMPS. It was also found that the χ increases faster than the Δu at early stages of cracking. A plateau is observed after about 15 h as some cracks merge with others one and no further opening is detected.

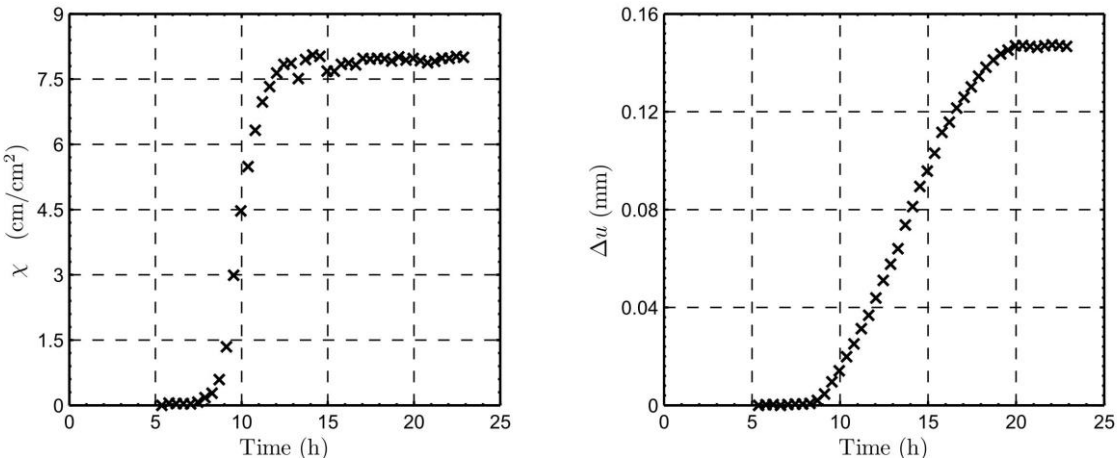

(a) (b)

Figure 7: (a) Time effect on the surface crack density, χ, and (b) average crack opening displacement, Δu.

4. Conclusion

As shown herein, it is possible to follow the development of crack networks with the help of the DIC method. The maximum principal strain fields were used to evaluate the average crack opening

displacement and the corresponding crack density during the curing and drying (CD) stages of refractory castables. The present technique is complementary to other ones quoted by Salomão et al. [2]. In further studies, based on its potential, the DIC will help to better understand the influence of physical effects (particle size, chemical analysis, temperature, etc.), which is low for early stages of curing and drying, but becomes much more relevant when hydration affects the bulk. It is also an interesting tool to validate numerical models that are developed to simulate the multiphysical phenomena involved in the CD stages.

5. Acknowledgments

The authors acknowledge the support from the National Council for Scientific and Technological Development (CNPq) and São Paulo Research Foundation (FAPESP), grant 2010/20927-3.

References

[1] Lee W, Moore R. Evolution of in situ refractories in the 20th century. Journal of the American Ceramic Society, 1998, 81(6):1385-1410

[2] Salomão R, Bittencourt L, Pandolfelli, V C. A novel approach for magnesia hydration assessment in refractory castables. Ceramics International, 2007, 33(5): 803-810

[3] Sutton M A, Zhao W, McNeill S R, et al. Helmcal crack closure measurements: development of a measurement system using computer vision and a far-field microscope. In: McClung R C, Newman Jr J C, ed. Advances in fatigue crack closure measurement and analysis: Second Volume, West Conshohocken: ASTM STP 1343, 1999.145-156

[4] Hild F, Roux S. Digital Image Correlation. In: Optical Methods for Solids Mechanics. A full-field approach, Weinheim (Germany): Wiley-VCH, 2012.183

[5] Robert L, Nazaret F, Cutard T, et al. Use of 3-D digital image correlation to characterize the mechanical behavior of a fiber reinforced refractory castable. Experimental Mechanics, 2007, 47(6):761-773

[6] Belrhiti Y, Germaneau A, Doumalin P, et al. Characterization of the mechanical behavior of magnesia spinel refractories using image correlation. Proceedings of the Unified International Technical Conference on Refractories (UNITECR 2013), Victoria, 2013, 4p.

[7] Rupil J, Roux S, Hild F, et al. Fatigue microcrack detection with digital image correlation. The Journal of Strain Analysis for Engineering Design, 2011, 46(6):492-509

[8] Mauroux T, Benboudjema F, Turcry Ph, et al. Study of cracking due to drying in coating mortars by digital image correlation. Cement and Concrete Research, 2012, 42(7):1014-1023

[9] G. Besnard, F. Hild, and S. Roux. "Finite-element" displacement fields analysis from digital images: Application to Portevin-Le Châtelier bands. Experimental Mechanics, 2006, 46(6):789-803

[10] Wattrisse B, Chrysochoos A, Muracciole J-M, et al. Analysis of strain localization during tensile tests by digital image correlation. Experimental Mechanics, 2001,41(1):29-39